Geochemistry of Main Types of Gold Deposits in Shear Zones, China*

WU XUEYI (吴学益), YANG YUANGEN (杨元根), XIAO HUAYUN (肖化云), AND WU HUIMING (吴惠明)

(*Open Laboratory of Ore Deposit Geochemistry, Institute of Geochemistry, Chinese Academy of Sciences, Guiyang* 550002, *China*)

Abstract: Shear zone-hosted gold deposits in China can be divided into four types: ductile, brittle-ductile, ductile-brittle and brittle, of which the ductile and brittle types are the basic ones. All these types of gold deposits have their own geochemical characteristics. The Hetai gold deposit in Guangdong Province, for example, is a mylonite-type gold deposit in a ductile shear zone. With increasing mylonitization, obvious changes took place in trace elements in minerals and rocks, enriching gold and mineralizing elements. The S and Pb isotope data indicated that the ore-forming materials were derived from the strata. Hydrogen and oxygen isotopic and fluid inclusion studies also implied that the ore-forming fluid was much closer to meteoric water from the early to the late ore-forming stage. The Linglong gold deposit, Shangdong Province, is a quartz-type gold deposit in a brittle shear zone. Changes in rocks, minerals and trace elements occurred in the process of formation of gold quartz veins, and the analytical results of S, Pb, H and O isotopes showed that ore deposition is connected not only with the Jiaodong Group, but also with anatexic granites.

Key words: shear zone; types of gold ore deposits; geochemical characteristics

Shear zone-hosted gold deposits in China can be divided into four types, i.e., ductile, brittle-ductile, ductile-brittle and brittle (Wu Xueyi, 1996, 1999) (Fig. 1), each of which has its own geochemical characteristics and is the product of crustal evolution in different stages.

Geochemistry of Ductile Shear Zone-Hosted Gold Deposits—Taking the Hetai Gold Deposit for Example

Characteristics of the rocks and minerals

With increasing intensity of ductile deformation, feldspar and biotite obviously decreased in contents, but quartz and sericite increased, as listed in Table 1.

Table 1. Minerals in different rocks in the Hetai gold deposit(%)

Sample	No. of samples	Quartz	Muscovite	Biotite	Albite	Microcline	Sericite
Metamorphic rock	8	35	20	25	15	5	
Migmatite	12	25	5	10	30	30	
Mylonitized migmatite	5	35	10	20	20	15	
Mylonite	3	45		<10	10	10	25
Phyllonite	5	40	10	5	5		40
Ultramylonite	5	75	5		1-2		20

ISSN 1000-9426

* This research project was financially supported by the National Natural Science Foundation of China (Nos. 49573189, 49403043) and the Key Gold Project of Chinese Academy of Sciences.

Chemical composition of the rocks

With increasing mylonitization, the contents of SiO_2 in the rocks increased obviously, but those of Al_2O_3, TiO_2, ΣFe, MgO and Na_2O+K_2O decreased obviously, as listed in Table 2.

Trace elements

The analytical results show that the contents of the trace elements including Au, Ag, Cu, Zn, As, Sb, Co, Ni, Sn, Be, B and Ba vary from high, low to high with increasing deformation intensity from metamorphic rock through migmatite to mylonite. Bi changed oppositely; Pb decreased in contents; Hg and Mo increased to some degree; Au, Ag and Cu increased in contents with increasing mylonitization intensity, as listed in Table 3.

Sulphur isotopes

The analytical results are given in Table 4. $\delta^{34}S$ values for the whole western region of Guangdong vary over a small range, indicating sulfur isotopic homogenization in the strata; the $\delta^{34}S$ values of phyllonite and ore samples are consistent with those of the strata in the western region of Guangdong, implying that the sulfur in ore-forming fluid has a close relationship with the strata.

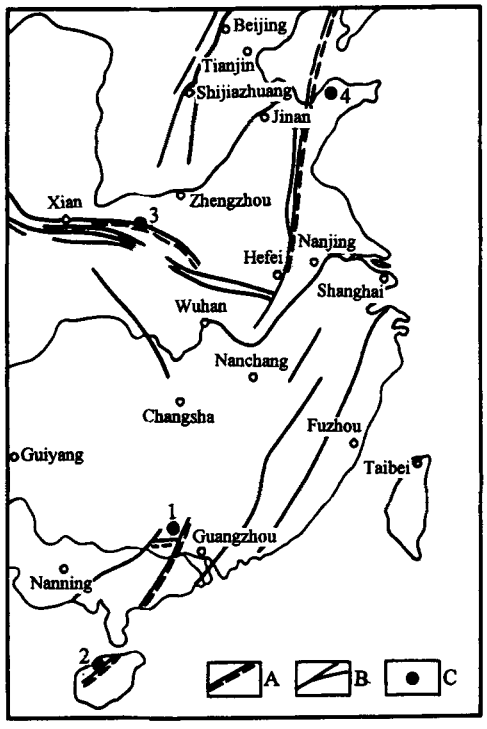

Fig. 1. Geological sketch map showing the distribution of the main types of shear zone-hosted gold deposits in China. A. Main shear zone; B. main fault; C. main types of shear zone-hosted gold deposits. 1. Hetai gold deposit; 2. Erjia gold deposit; 3. Shanggong gold deposit; 4. Linglong gold deposit.

Table 2. Chemical analyses of the rocks in the Hetai gold deposit(%)

Sample	Metamorphic rock	Migmatite	Mylonite	Phyllonite	Silicified ore
No. of samples	3	13	5	5	2
SiO_2	65.72	70.35	70.87	74.06	78.75
Al_2O_3	17.72	15.30	13.45	12.24	4.13
TiO_2	0.63	0.36	0.43	0.41	0.25
Fe_2O_3	1.62	0.55	2.38	0.63	6.12
FeO	4.14	3.78	3.82	2.78	1.61
MnO	0.04	0.10	0.11	0.04	0.01
MgO	2.07	1.43	1.35	1.35	2.09
CaO	0.25	1.93	1.15	0.89	0.11
Na_2O	0.75	2.99	1.82	1.15	1.38
K_2O	4.20	3.09	3.35	3.66	3.00
P_2O_5	0.16	0.01	0.14	0.11	0.02

Table 3. Trace element composition of the Hetai gold deposit ($\times 10^{-6}$)

Sample	No. of samples	Au($\times 10^{-9}$)	Ag($\times 10^{-9}$)	Cu	Pb	Zn	Mo	As	Sb
Schist	5	15.17	157.71	29.97	39.76	76.08	0.70	20.77	0.31
Migmatite	8	14.31	148.38	26.86	36.88	40.25	0.89	5.70	0.15
Mylonite	37	261.8	343.3	339.2	17.17	43.25	0.98	12.01	0.38
Sample	No. of samples	Bi	Hg	Co	Ni	Sn	Be	B	Ba
Schist	5	1.06	0.016	12.87	24.51	18.31	2.61	75.83	407.5
Migmatite	8	1.82	0.018	6.43	17.1	14.21	1.51	48.4	313
Mylonite	37	0.77	0.024	12.07	21.88	19.22	2.97	59.17	541.2

Table 4. Sulfur isotopic composition of the Hetai gold deposit (‰)

Sample	Phyllonite	Ore							West Guangdong, China
Mineral measured	Pyrite	Pyrite	Chalcopyrite	Pyrrhotite	Galena	Sphalerite	Average		
No. of samples	3	21	7	2	5	3	3	8	
$\delta^{34}S$	-2.34 - 1.83	-3.06 - 1.48	-2.32 - 1.32	-2.36 - 2.28	-8.19 - 1.35	-4.54 - 3.16	early	late	
Average	-1.92	-2.91	-2.00	-2.32	-5.63	-1.97	-2.00	-4.26	-3 - 3

Lead isotopes

Many scientists have studied the lead isotopic composition of the Hetai gold deposit (Table 5). It is obvious that from the old crystallization basement, magmatic activity during the Hercynian to Indosinian movements and ductile shear zone activity to the ore-forming process, lead isotopic values showed an evolution trend of being highest to lowest and higher to lower, but generally speaking, the lead isotope values of ores are close to those of the Sinian strata(Zc).

Table 5. Lead isotopic composition of the Hetai gold deposit (‰)

Sample		Material measured	$^{206}Pb/^{204}Pb$	$^{207}Pb/^{204}Pb$	$^{208}Pb/^{204}Pb$
Ore		Quartz	18.248 - 19.184 18.659(11)	15.559 - 15.762 15.666(11)	38.138 - 39.477 38.794(11)
		Sulfide	17.919 - 19.078 18.684(15)	15.548 - 15.790 15.695(15)	38.013 - 39.052 38.868(15)
Tectonite		Whole rock	18.715 - 19.025 19.017(3)	15.701 - 15.771 15.730(3)	39.411 - 39.489 39.438(3)
Migmatite			18.786 - 19.133 18.940(4)	15.734 - 15.780 15.756(4)	39.833 - 39.177 39.051(4)
Sinian Formation		Metamorphic rock	18.970 - 19.290 19.097(3)	15.837 - 15.947 15.877(3)	38.320 - 38.520 38.410(3)
Granite	Granite-pegmatite	Potash feldspar	18.420 - 19.189 18.737(3)	15.680 - 15.719 15.699(3)	38.726 - 38.753 38.742(3)
	Wucun granite	Potash feldspar	18.532 - 18.973 18.758(3)	15.613 - 15.730 15.68(3)	38.656 - 39.124 38.920(3)
	Yunlougang granite	Potash feldspar	18.402 - 18.902 18.531(5)	15.690 - 15.788 15.712(5)	38.472 - 38.939 38.750(5)

Note: No. of samples is in the bracket. From Zhang Zhilan (1989); the No. 719 Team of Geology and Exploration of Guangdong, China (1988); Liu Jianjun (1990).

H and O isotopes in the Hetai gold deposit

The analytical results are presented in Table 6. The H and O isotope values of the Yunlougang rock body are close to those of metamorphic water while those of the Wucun rock body

are similar to those of magma water, and their isotope values are significantly different from those of ores. The isotope data for mylonitic migmatite are within the range of ores, and from the early stage to the late stage, the isotopic composition is much closer to that of meteoric water. So it is inferred that the ore-forming fluid was derived from circulating heated-aqueous fluid from meteoritic water.

Table 6. Hydrogen and oxygen isotopic composition of the Hetai gold deposit (‰)

Sample	Mineral measured	$\delta^{18}O_{H_2O}$	δD
Yunlougang magmatic rock	Quartz	+10.1	−57.0
Wucun magmatic rock	Quartz	+11.1	−65.0
Mylonitized migmatite	Quartz	+6.18	−77.1
Silicified phyllonite	Quartz	−5.21 − +7.61	−81.5 − −56.9
Gold-bearing quartz vein	Quartz	−4.52 − +8.04	−80.2 − −54.0
Sulfide-rich calcite vein	Calcite	−4.2 − −2.2	−56 − −49

From the No.719 Team of Geology and Exploration of Guangdong, China (1988); Liu Jianjun (1993); and Zhuang Longchi (1988).

Characteristics of fluid inclusions

The fluid inclusions can be divided into three groups: 1) dark-coloured gaseous inclusions, with a ratio of gas to liquid of 75%, measuring 001 − 0.01 mm in size; 2) gaseous-liquid inclusions with a ratio of gas to liquid of less than 50%, measuring 0.004 − 0.02 mm in size; and 3) pure liquid inclusions, distributed along cracks, and less than 0.001 mm in size. This implies the mixing characteristics at different stages.

Geochemical Characteristics of Brittle-Ductile Shear Zone-Hosted Gold Deposits—Taking Erjia Gold Deposit for Example

Petrochemical-chemical analyses of the rocks

The petrochemical and chemical analyses of the rocks are presented in Table 7. From this table we can see that with increasing mylonitization the contents of SiO_2 and gold increased, and those of gold also increased with increasing oxidation degree. The lower the Fe^{3+}/Mg^{2+} ratio is, the higher the content of gold in the rocks will be.

Table 7. Chemical analyses of the rocks in the Erjia gold deposit (%)

Sample	Migmatite	Mylonitized migmatite	Catalastic migmatite	Mylonite	Ultramylonite
Sample No.	P10-1	P3-4	88-7-8	88-7-10	88-7-7
SiO_2	68.80	70.60	63.44	64.29	75.12
TiO_2	0.40	0.09	0.97	0.71	0.55
Al_2O_3	14.68	17.43	17.66	16.74	11.92
Fe_2O_3	0.43	0.06	3.86	4.54	1.84
FeO	3.32	0.57	1.64	0.96	1.17
MnO	0.06	0.01	0.02	0.01	0.01
MgO	0.90	0.30	1.10	0.70	0.20
CaO	2.20	0.20	0.20	0.10	0.10
Na_2O	2.90	6.04	2.36	2.09	3.45
K_2O	4.19	3.29	6.39	5.93	3.39
H_2O^+	1.09	0.95	1.94	1.48	0.98
H_2O^-	0.05	0.001	0.05	0.05	0.001
P_2O_5	0.08	0.01	0.27	0.31	0.36
S				1.25	
Total	99.12	99.55	99.90	99.16	99.09

Trace elements

The analytical results of trace elements are given in Table 8. It is obvious that the contents of Cu, Pb, Zn and Sn in the ore increase with increasing gold content. Ag, As and Fe also increase in contents. The contents of As, Pb and Zn increase obviously and those of Ag and Cu also increase, but slightly, from wall rock through pre-mylonite and mylonite to ultramylonite (ore body), indicating that some of the Cu, Pb, Zn, Au and Ag in the ore were derived from the strata.

Table 8. Contents of trace elements in the rocks and ores in the Erjia gold deposit ($\times 10^{-6}$)

Sample No.	Sample	Au	Ag	Cu	Pb	Zn	Fe	As	Sb	W
Q7-10	Altered migmatitic schist	0.830	11.04	10	67	236	28000	7500	1	10
88-10-1	Altered mylonite	0.400	0.01	36	2	143	26880	21100	0.6	7
Q7-9	Altered migmatite	0.049	0.92	15	67	241	24150	100	1	4
23	Altered sericite schist	0.046	0.01	18	19	110	27440	22	0.8	4
25	Altered phyllite	0.015	0.50	10	19	65	25760	20	0.8	2
Q3-4	Altered migmatitic schist	0.014	0.01	6	2	220	23100	14	0.30	4
24	Altered ultramylonite	0.012	0.50	12	39	15	18410	9700	0.30	1
V17-9-6	Ore	40.10	0.92	96	500	444	10500	390	30	182
Q7-11	Quartz vein	12.0	0.72	15	100	218	11200	2800	10	3
V17-10-7	Ore	7.63	0.14	15	67	238	21350	6100	5	52
V17-7-01	Ore	3.0	0.20	25	300	477	8400	900	12	2

Rare-earth elements

The contents of rare-earth elements and their distribution patterns are listed in Table 9 and shown in Fig. 2, respectively. The analytical results show: 1) in gold ores, the contents of REE decrease with increasing gold content; 2) ore migmatite, metamorphic rock and mylonite samples have similar REE distribution patterns, indicating that the ore-forming materials may have come from the strata; on the other hand, diorite-porphyrite samples also have the same REE distribution patterns as the ore samples, and also have similar Eu anomalies. This also evidences that the ore-forming materials have relationships not only with the strata, but also with the magma which is of the same origin as the diorite-porphyrite.

Sulphur isotopes

Sulfur isotopic analyses are given in Table 10. From this table we can see that sulfur isotope values lie mainly between 4.3 ‰ and 6.0 ‰ and are normally distrbuted with increasing mylonitization from migmatite to pre-mylonite and mylonite. $\delta^{34}S$ values are given in Table 10.

Lead isotopes

We can see from Table 11 that: 1) From metamorphic rock→migmatite→migmatitic gneiss→early-stage ore (pyrite)→diorite porphyrite→late-stage ore (galenite), the lead isotope values decrease obviously and μ values also show the same variation trend. This gives us an idea that the lead may be derived from the paleo-crystallization basement. 2) Lead isotopic composition of ores varies over a large range. This implies that the lead became homogenized during the ore-forming process. 3) All the samples have higher μ values, which implies an abnormal lead source, i.e.,, uranium-rich strata, as can be seen in Zartman's projection diagram.

Table 9. Chemical analyses of rare-earth elements in the Erjia gold deposit ($\times 10^{-6}$)

Sample type	Migmatite	Migmatitic schist	Mylonitized migmatitic schist	Mylonitized schist	Ultra-mylonite	Mineralized mylonite	Granite pegmatite	Por-phyritic granite	Diorite	Mineralized quartz vein	Ore
Sample No.	P10-1	P10-2	Baoban Group	SV11-1-1	SV11-1-3	V17-7-d	88-2-3	88-12-3	Q7-12-2	Q7-11	V7-11
La	38.32	45.82	15.66	49.46	7.04	11.78	16.45	57.58	42.76	$Re_2O_3=$	$Re_2O_3=$
Ce	69.73	83.58	30.66	91.48	14.95	24.02	29.93	91.27	76.82	36×10^{-6}	36×10^{-6}
Pr	8.22	9.96	3.11	9.36	2.03	3.05	3.55	9.91	9.01		
Nd	32.84	39.2	12.19	43.97	9.02	13.74	14.53	35.18	35.13		
Sm	7.20	8.42	2.66	9.60	2.34	3.12	3.14	5.05	6.63		
Eu	1.12	1.38	0.22	0.12	0.28	0.74	0.74	1.27	0.78		
Gd	8.37	9.74	1.78	9.11	2.78	3.48	3.38	4.23	4.73		
Tb	1.34	1.17	0.26	1.28	0.50	0.50	0.55	0.62	0.60		
Dy	9.16	11.5	1.48	7.32	3.10	2.90	3.74	3.62	2.93		
Ho	1.76	2.50	0.28	1.36	0.65	0.59	0.79	0.64	0.47		
Er	5.04	6.90	0.81	3.19	1.79	1.31	2.27	1.60	1.10		
Tm	0.75	1.05	0.12	0.43	0.27	0.16	0.43	0.21	0.13		
Yb	5.06	6.58	0.82	2.66	1.91	0.82	2.05	1.18	0.55		
Lu	0.76	1.06	0.16	0.37	0.30	0.10	0.34	0.21	0.08		
ΣREE	189.7	228.98	70.12	229.71	48.94	66.31	81.53	212.6	181.72		
L/HREEE	4.88	4.65	11.30	7.93	3.16	5.13	5.06	16.27	16.16		
δEu	-0.55	-0.53	-0.69	0.96	-0.66	-0.31	-0.55	-0.15	-0.57		
Au	0.093	0.096				3	0.013	0.013		12.0	48.1

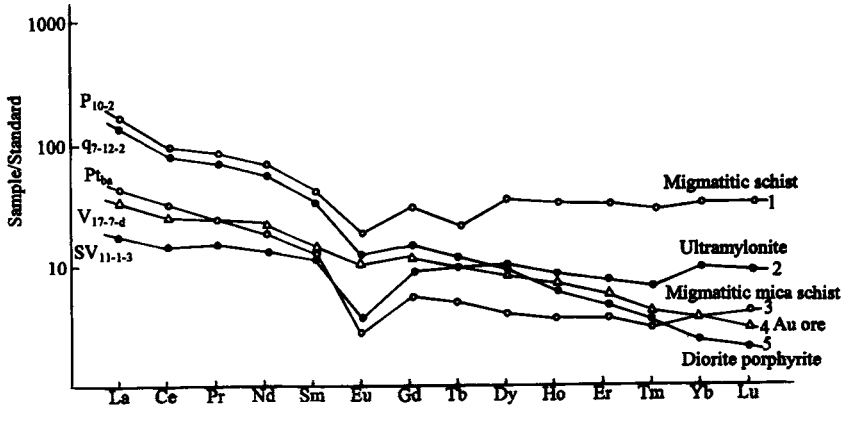

Fig. 2. The REE distribution patterns in the Erjia gold deposit. 1. Migmatitic schist; 2. ultramylonite; 3. migmatitic muscovite schist; 4. gold ore; 5. diorite-porphyrite.

Fluid inclusions

Homogenization temperatures of inclusions for the three different stages are presented below: quartz-pyrite, arsenopyrite stage, 300 – 350℃; polymetal sulfides-quartz-natural gold stage, 250℃; calcite-quartz stage, 200℃. The ore-forming pressure ranges from 200×10^5 Pa to 500×10^5 Pa. As can be seen from Table 12, the inclusions in silicified ores are characterized as being rich in K^+, Na^+, SO_4^{2-} and HCO_3^-; those in quartz veins, K^+, Na^+, Ca^{2+}, SO_4^{2-}, HCO_3^- and Cl^-, while calcite veins, Ca^{2+} and HCO_3^-. Ore-forming fluids were rich in CO_2, CH_2 and H_2O in the early and middle stages of ore-forming process.

Geochemistry of Ductile-Brittle Shear Zone-Hosted Gold Deposits—Taking the Shanggong Gold Deposit, Henan Province for Example

Abnormality

Au and Ag show obvious abnormalities and Pb, Zn, Cu, As, Mn and (Mo, Co) in hydrothermal sediments show obvious mixed abnormalities which extend in the same direction as the tectonic alteration belt.

Table 10. Sulfur Isotopic composition of the Erjia gold deposit (‰)

Sample No.	Mineral measured	Sample type	$\delta^{34}S$	Sample No.	Mineral measured	Sample type	$\delta^{34}S$
V11-1-2	Pyrite	Silicified schist	4.37	V17-10-6	Arsenopyrite	Silicated schist	3.78
V11-1-3	Pyrite	Silicified migmatite	6.03	HL_{87}-57	Pyrite	Migmatitic gneiss	2.41
V11-1-4	Pyrite	Migmatitic gneiss	4.46	HL_{87}-66	Pyrite	Siliceous rock	6.45
V11-5-4	Arsenopyrite	Silicified schist	6.80	HL_{87}-67	Pyrite	Silicated migmatite	6.08
V17-7-A	Pyrite	Silicified migmatite	8.18	HL_{87}-70	Pyrite	Quartz vein	6.55
V17-7-5-1	Pyrite	Siliceous rock	4.87	Jia1	Pyrite	Migmatitic gneiss	4.35
V17-7-3-2	Pyrite	Silicified chlorite-schist	5.39	Jia2	Pyrite	Migmatitic gneiss	5.09
V17-7-4	Pyrite	Gneiss	5.16	Jia5	Pyrite	Silicated migmatitic schist	4.90
V17-9-4	Pyrite	Siliceous rock	5.55	Jia10	Pyrite	Silicated gneiss	3.68
V17-9-4-3	Pyrite	Siliceous rock	3.74	Jia88-1	Pyrite	Mylonite	8.26
V17-9-5	Pyrite	Siliceous rock	9.76	Jia88-2	Pyrite	Siliceous rock	1.85

Table 11. Lead Isotopic composition of the Erjia gold deposit (‰)

Sample type	Material measured	$^{206}Pb/^{204}Pb$	$^{207}Pb/^{204}Pb$	$^{208}Pb/^{204}Pb$	μ
Ore	Pyrite	18.677 – 19.286 18.992(7)	15.480 – 16.027 15.768(7)	38.919 – 40.464 39.627(7)	9.2 – 10.2 9.75
	Galena	18.646	15.591	38.649	9.4
Diorite-porphyrite	Pyrite	18.824	15.691	39.087	9.6
Migmatitic gneiss	Rock	19.246 – 19.299 19.273(2)	15.644 – 15.656 15.650(2)		
Migmatite	Rock	19.189 – 19.723 19.510(3)	15.542 – 15.803 15.682(3)	38.720 – 40.072 39.26(3)	9.5 – 9.9 9.73(3)
Muscovite-rich quartz schist	Rock	20.178 – 28.113 21.646(2)	15.776 – 16.185 15.980(2)	42.632 – 45.091 48.826(2)	10.0 – 11.3 10.65(2)

Note: In the bracket is the No of samples.

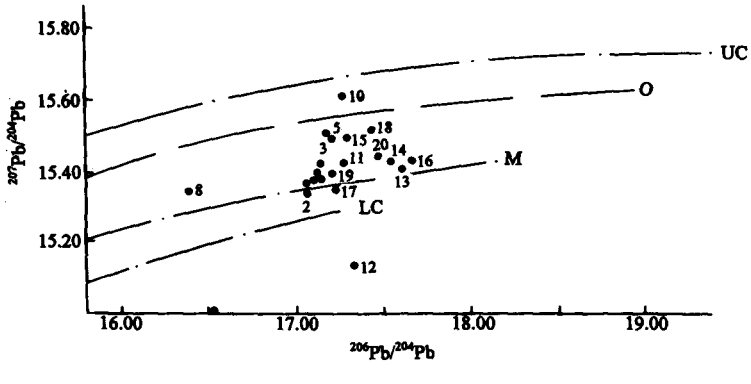

Fig. 3. Lead isotope model of the Shanggong gold deposit and its adjacent occurrences (after Doe and Zartman,). The numbers in the Figure are the sample Nos.

Table 12. Compositions of inclusions in quartz from the Erjia gold deposit (μg/g)

Mineralization stage		I	II			III	
Sample No.		17-9-6	Q3-1	Q4	Q9-1	CC2	CC1
Vapor component	H_2O	825	1520	1280	1040	340	530
	CO_2	11.3	77.8	84.9	64.3	8.0	5.8
	H_2	0.146	0.0301	0.0584	0.0716	0.0697	0.039
	O_2	–	–	–	–	–	–
	N_2	0.9	2.2	1.4	1.6	0.5	0.5
	CO	1.0	1.3	1.0	1.7	–	–
	CH_4	0.23	1.55	1.35	2.05	0.09	0.08
	C_2H_6	–	0.7	0.6		–	–
Liquid component	F^-	0.86	1.03	1.15	0.30	1.26	1.03
	Cl^-	2.34	2.34	4.68	2.03	3.19	2.55
	SO_4^{2-}	21.54	1.54	1.92	5.77	16.92	1.46
	Na^+	4.54	2.69	4.69	1.23	1.08	1.46
	K^+	11.73	1.35	2.31	3.85	0.38	0.48
	Ca^{2+}	2.06	1.94	1.83	2.29	51.5	50.01
	Mg^{2-}	0.50	0.07	0.10	0.20	2.61	0.70
Metallic component	Au	0.09	0.06	0.05	0.10	trace	trace
	Ag	0.18	0.10	0.11	0.14	0.06	0.07
	Fe	0.36	0.18	0.27	0.18	0.45	0.36

Table 13. Sulfur isotopic composition of the Shanggong gold deposit

Sequence No.	Sample	Mineral measured	$\delta^{34}S$ ‰	Ref.
1	Cubic pyrite disseminated in altered andesite(I)	Pyrite	+4.18	⑤
2	Cubic pyrite disseminated in altered andesite(I)	Pyrite	+4.06	⑤
3	Pyrite in quartz vein(I)	Pyrite	+3	②
4	Breccioid ore	Pyrite	−11.25	①
5	Ore	Pyrite	−13.18	③
6	Ore	Pyrite	−10.96	③
7	Fine-grained pentagonal-dodecahedral pyrite in ore	Pyrite	−11.98	⑤
8	Fine-grained pentagonal-dodecahedral pyrite in andesite	Pyrite	−14.46	⑤
9	Fine-grained pentagonal-dodecahedral pyrite in ore	Pyrite	−10.90	⑤
10	Fine-grained pentagonal-dodecahedral pyrite in ore	Pyrite	−7.84	⑤
11	Fine-grained pentagonal-dodecahedral pyrite in ore	Pyrite	−6.54	⑤
12	Fine-grained pentagonal-dodecahedral pyrite in ore	Pyrite	−11.34	⑤
13	Fine-grained pentagonal-dodecahedral pyrite in ore	Pyrite	−10.49	⑤
14	Fine-grained pentagonal-dodecahedral pyrite in ore	Pyrite	−10.57	⑤
15	Fine-grained pentagonal-dodecahedral pyrite in ore	Pyrite	−13.12	⑤
16	Sulfide-rich breccioid ore	Galena	−16.62	⑤
17	Galena-rich ore	Galena	−15.88	⑤
18	Ankerite-rich ore	Galena	−19.24	⑤
19	Ore	Galena	−16.97	⑤
20	Ore	Galena	−12.98	⑤
21	Ore	Galena	−19.20	⑤
22	Galena-rich breccioid ore	Galena	−13.39	⑤
23	Disseminated sulfide-rich ore	Galena	−14.53	⑤
24	Ore	Barite	−0.54	⑤
25	Gold-bearing sulfide quartz vein	Chalcopyrite	+6.68	⑤
26	Sulfide-rich ore	Pyrite	+6.02	⑤
27	Sulfide-rich ore	Galena	+0.78	⑤
28	Ore (III)	Galena	+1.51	⑤
29	Xiong'er Group volcanic rock	Pyrite	+3.6	②
30	Huashan granite	Pyrite	+2.3	②
31	Archaean gneiss	Pyrite	+1.92	④

From ① Chen Yanjing (1992); ② Zhao Rui (1989); ③ Institute of Geology of Henan, China (1985); ④ Wang Hengzhi (1985); ⑤ No. 1 Regional Team of Geology and Exploration of Henan, China (1988).

Major and trace elements

Correlation analysis show that Au has a positive correlation with Ni, Yb, K, Na, Mg and Fe, but has an obviously negative correlation with the elements Cu, Pb, Zn, F, Cl, Ca, etc.

Sulphur isotopes

Sulphur isotopic analyses are presented in Table 13. From this table we can see that $\delta^{34}S$ values are within the range of $+6.6‰ - -19.24‰$, showing great variations at different ore-forming stages. This indicates that the source of sulphur was complicated and the physical-chemical conditions of ore deposition varied to a great degree.

Lead isotopes

As you can see from Table 14 and Fig. 3, the lead isotope data for the Shanggong gold deposit and the Huashan rockbody fall between the mantle line and the orogeny belt, indicating that the lead in the ore is a mixed lead of diverse origin.

Table 14. Lead isotopic composition of rocks and ores in the Shanggong gold deposit

Sample No.	Sample type	Sampling location	$^{206}Pb/^{204}Pb$	$^{207}Pb/^{204}Pb$	$^{208}Pb/^{204}Pb$	μ	Th/U	Ref.
$Sg\text{-}Pd_3\text{-}Pb\text{-}Tz_1$	Galena-rich ore	$ShangPd_3CM_4$	17.095	15.378	37.502	8.06	4.12	①
Tz_3/Pd_3	Disseminated galena-rich ore	$ShangPd_3CM_4$	17.053	15.344	37.417	8.01	4.09	①
$SgPd_3DF_2Pb$	Breccioid galena-rich ore	$ShangPd_3CM_4$	17.208	15.503	37.949	8.27	4.30	①
Rz_2/Pd_3		$ShangPd_3CM_4$	17.105	15.384	37.558	8.07	4.14	①
Rz_3/Pd_3		$ShangPd_3CM_4$	17.188	15.508	37.938	8.28	4.31	①
Rz_1/Pd_6		$ShangPd_6$	17.119	15.393	37.566	8.08	4.14	①
$SgPd_1YM_1$	Galena-rich ankerite vein	$ShangPd_1$	17.085	15.367	37.474	8.04	4.11	①
$Sg\text{-}Pd_{20}\text{-}DF_1\text{-}Pb$	Sulfide-rich ore	$ShangPd_{20}$	16.378	15.355	36.426	8.12	4.04	①
$GS\text{-}DF_1\text{-}Pb$	Breccioid galena-rich ore	Qianshu	17.136	15.402	37.642	8.10	4.17	①
Shang-30	Sulfide-rich ore	Shanggong	17.283	15.615	38.168	9.66	4.58	②
$Q1\text{-}DF_2\text{-}Pb$	Galena-rich ore	Qiliping	17.273	15.420	37.677	8.12	4.09	①
Luo-4	Sulfide-rich ore	Qiliping	17.344	15.136	37.971	8.66	4.34	②
Luo-5	Sulfide-rich ore	Qiliping	17.615	15.406	38.024	9.17	4.21	②
Luo-22	Sulfide-rich ore	Congyanggou	17.545	15.437	37.95	9.246	4.27	②
Luo-27	Sulfide-rich ore	Congyanggou	18.289	15.502	38.415	9.279	4.03	②
Luo-31	Sulfide-rich ore	Congyanggou	17.699	15.429	37.984	9.209	4.18	②
W-DF-1/1	Galena-rich ore	Weijiagou	17.226	15.344	37.295	7.99	3.92	①
H-Pb-1	Potash feldspar in granite	Huashan	17.44	15.520	37.975	8.27	4.16	①
H-Pb-2	Potash feldspar in granite	Huashan	17.199	15.391	37.447	8.07	4.03	①
H-Pb-3	Potash feldspar in granite	Huashan	17.473	15.455	37.886	8.16	4.07	①

Note: ① The No. 1 Regional Team of Geology and Exploration of Henan (1988); ② Institute of Geology of Henan (1985).

Carbon isotopes

As can be seen from Table 15, the $\delta^{13}C$ values of five dolomite samples vary over a narrow range, indicating a single source of carbon. The $\delta^{13}C$ values are close to those of marine carbonates, indicating the carbon was derived from carbonate strata, that is, from the Shuidigou rock series in the basement composed of metamorphic rocks.

H and O isotopes

As seen from Table 16, the $\delta^{18}O$ values of ores and altered rocks are obviously higher than

those of unaltered volcanic rocks of the Xionger Group, indicating that the ore-forming fluid is of metamorphic hydrothermal or magmatic hydrothermal origin.

Table 15. Carbon isotopic composition of ankerite in the Shanggong gold deposit

Sample No.	Sample	$\delta^{13}C$ (‰)
Sg-Pd_1-C-DF_1	Moderate-coarse grained ankerite vein	-2.20
Sg-Pd_1-YM_1-CM_4-C-2/1	Galena-rich ankerite vein	-1.58
Sg-Pd_1-YM_1-B_t-2	Ankerite vein	1.51
Sg-Pd_2-CM_6-DF_1-0	Ankerite-rich quartz vein	-1.85
GS-DF_2-0	Ankerite banded material in ore	0.03

From the No. 1 Regional Team of Geology and Exploration of Henan, China.

Table 16. Hydrogen and oxygen isotopic compositions of rocks, ores and mineraling fluids in the Shanggong gold deposit

Sequence No.	Sample	Mineral or rock	$\delta^{18}O$(‰)	T(℃)	$\delta^{18}O_{liq.}$(‰)	$\delta D_{liq.}$(‰)	Ref.
1	Phacoidal quartz vein	Quartz	15.47	250-360	6.09-9.93		④
2	Quartz fragment in breccioid ore	Quartz	14.26	260-350	5.33-8.45		④
3	Quartz vein	Quartz	11.19	315±	4.34		④
4	Quartz vein	Quartz	11.68	358	6.09	-79.3	④
5	Quartz vein	Quartz	10.42	330	4.83		④
6	Quartz vein	Quartz	10.67	375	4.29		④
7	Quartz vein	Quartz	10.39	351	5.23		④
8	Ore	Quartz	12.21	326	6.43	-72.8	④
9	Ore	Quartz	16.67	326	10.17	-82.6	④
10	Ore	Quartz	15.72	321	9.22	-66.4	④
11	Ore	Quartz	15.10	328	3.44	-87.6	④
12	Ore	Quartz	14.10	360	7.57	-83.7	④
13	Ore	Quartz	17.93	210-240	12.39		④
14	Bruiachite	Bruiachite				-56.4	④
15	Dolomitized andesite	Rock	6.65				④
16	Ankerite-rich andesite	Rock	8.65				④
17	Pyrite-rich ore	Rock	12.65				④
18	Andesite	Rock	7.46			-82.5	①
19	Andesite	Rock	7.79				④
20	Ankerite-rich andesite	Rock	8.87			-85.4	①
21	Amygdaloidal andesite	Rock	8.49			-94.0	①
22	Amygdaloidal ankerite-rich andesite	Rock	11.24			-87.1	①
23	Ore	Quartz	15.27	318	8.55		②
24	Ore	Quartz	15.79	318	9.07		②
25	Quartz vein	Quartz	11.7	330	5.36		③
26	Quartz vein	Quartz	12.6	330	6.26		③
27	Ankerite vein	Ankerite	10.19	200	0.085		④
28	Ankerite vein	Ankerite	10.60	160-200	-1.90-0.50		④
29	Ankerite vein	Ankerite	13.13	145	-0.58		④
30	Ankerite vein	Ankerite	11.66	290-320	5.34-6.24	-75.6	④
31	Ankerite banded-material in breccioid ore	Ankerite	15.09	288	8.17	-66.9	④

① Li Shimei (1989); ② Institute of Geology of Henan, China (1985); ③ Chen Yanjin (1992); ④ No. 1 Regional Team of Geology and Exploration of Henan, China (1988).

Fluid inclusions

The features of inclusions and the inclusion composition analytical results for the Shanggong gold deposit are given in Table 17 (Chen Yanjin, 1992).

Table 17. Chemical compositions of fluid inclusions from the Shanggong gold deposit

No.	1	2	3	4	5	6	7	8	9	10	11	X1	X2	X3
Stage	Ⅱ	Ⅰ	Ⅰ	Ⅰ	Ⅰ	Ⅰ	Ⅰ	Ⅰ	Ⅲ	Ⅲ	Ⅲ	Ⅰ	Ⅱ	Ⅲ
K^+	4.37	6.00	3.67	7.24	4.55	1.30	2.20	2.55	4.85	2.65	2.30	5.34	2.02	3.27
Na^+	33.07	32.70	37.78	11.49	33.17	6.55	8.00	5.05	1.40	3.15	16.30	28.79	6.53	6.95
Ca^{2+}	15.10	11.00	10.89	23.86	12.59	15.00	17.15	12.9	6.35	18.95	16.10	14.59	15.02	13.80
Mg^{2+}	14.23	0.57	0.56	15.11	1.10	0.60	0.75	0.65	7.55	0.80	0.85	4.34	0.67	3.07
Fe^{3+}	3.74	0.86	0.78	0.37	0.60	0.60	1.00	0.65	1.60	4.50	1.85	0.65	0.65	2.65
Cu^{2+}		0.14	0.11											
Pb^{2+}					0.50									
Zn^{2+}	0.15	0.37	0.44	0.21	0.30									
HCO_3^-						36.25	22.60	9.70	27.65	36.75	36.50		23.18	33.63
F^-	2.87	1.86	2.33	2.62	2.00	0.70	0.75	0.80	1.50	0.37	0.42	2.20	0.75	0.76
Cl^-	53.04	37.84	46.11	43.09	45.95	9.10	14.15	12.75	2.60	2.00	3.10	43.25	12.00	2.57
SO_4^{2+}	87.36	1.43	2.22	0.62	5.00	6.10	7.20	4.75	6.10	3.70	9.10	2.32	6.02	6.30
CO						10.34	30.08	3.51	26.25	30.36	30.49		13.64	29.03
CH_4						0.057	0.23	0.059	0.36				0.115	0.12
CO_2						4.31	2.88	1.54	1.98	2.21	2.22		2.91	2.14
H_2O						19.05	18.94	10.61	10.20	14.01	13.33		16.35	12.51
ΣM^+	70.66	51.64	54.23	58.28	52.51	24.05	29.10	21.80	21.75	30.05	37.40	54.17	24.98	29.73
ΣM^-	143.27	41.43	50.66	46.33	52.95	52.15	45.70	28.00	37.85	42.82	49.12	47.84	41.95	43.26
ΣM^0						34.21	52.13	15.72	38.79	46.58	46.04		34.02	43.80
$\Sigma M^{\pm}$	213.93	93.07	104.9	104.6	105.5	76.20	74.80	49.80	59.60	72.87	86.62	51.01	33.47	36.50
pH	7.85	4.74	4.72	7.68	5.06	7.41	6.50	5.47	7.49	7.58	7.48	5.55	6.46	7.52
Eh	-9.41	174.6	175.8	0.65	155.7	16.63	70.46	131.39	11.89	6.57	12.49	126.7	72.83	10.32
EC						0.59	1.30	0.52	0.86	0.55	0.65		0.80	0.69
F/Cl	0.054	0.049	0.051	0.161	0.044	0.077	0.053	0.063	0.577	0.185	0.135	0.051	0.03	0.296
CO_2/H_2O						0.22	0.15	0.15	0.19	0.16	0.17		0.17	0.17
K/Na	0.132	0.183	0.097	0.630	0.137	0.198	0.275	0.505	3.464	0.841	0.141	0.262	0.326	1.482
K_n/M_c	1.274	3.172	3.620	0.481	2.755	0.503	0.570	0.561	0.450	0.293	1.097	2.507	0.545	0.613

From the analytical data of the researchers, we can conclude that the ore-forming temperatures at different stages are: stage Ⅰ, 320－360℃; stage Ⅱ, 220－320℃ and stage Ⅲ, 140－200℃, respectively. And the contents of Mg^{2+}, Fe^{3+}, Cl^-, SO_4^{2-}, ΣM^+, ΣM^- and ΣM in quartz inclusions of stage Ⅰ and in ferrodolomite inclusions of stage Ⅲ are much lower than those in brecciated ores of stage Ⅱ. This indicates that ore-forming solutions at stage Ⅱ would be more beneficial to mineralization.

Geochemistry of Brittle Shear Zone-Hosted Gold Deposits— Taking the Linglong Gold Deposit, Shandong Province, for Example

Chemical composition of the ore

The analytical results are given in Table 18. (Wang Jijun et al., 1991), Generally speak-

ing, gold ores of the sulfide-quartz vein type are poor in SiO_2 and Al_2O_3, and rich in Fe_2O_3, but veinlet disseminated gold ores of the sericite-quartzite type are rich in SiO_2, Al_2O_3, and poor in Fe_2O_3, and disseminated pyrite gold ores of the quartz vein type are rich in SiO_2 and Al_2O_3 and poor in Fe_2O_3 as compared with massive pyrite gold ores of the quartz vein type.

Table 18. Chemical analyses of ores in the Linglong gold deposit

Ore type	Sample	SiO_2	Al_2O_3	TiO_2	CaO	MgO	Fe_2O_3	FeO	MnO	K_2O	Na_2O	H_2O	S
Quartz vein	Massive pyrite-rich ore	41.6	2.1	0.2	0.4	0.2	30.6	2.8	0.02	0.8	0.1		
	Banded pyrite-rich ore	49.8	9.3	0.03	0.5	1.2	28.1	0.1	2.9	2.2	0.1	4.3	0.6
	Disseminated pyrite-rich ore	71.6	3.0	0.1	0.4	0.3	12.7	1.6	0.02	1.3	0.1		
Phyllic rock	Veinlet-disseminated pyrite-rich ore	65.8	12.6	0.4	0.7	0.8	8.2	0.9	0.03	4.2	1.3	2.6	5.0
	Veinlet-disseminated pyrite-rich ore	72.1	12.0	0.1	0.6	0.8	4.6	1.5	0.10	4.6	0.2	1.7	2.6
	Veinlet-disseminated pyrite-rich ore	73.1	12.9	0.2	0.5	0.7	4.4	0.7	0.06	4.1	2.4	1.3	0.1

Trace elements

Eleven trace elements have been analyzed in ore quartz and ore-barren quartz, and the results show that nine of the elements show the following variation trends: quartz in ore quartz vein is rich in Sb, Sr, Ba, Ni and Zn, and poor in Cr, Mn, and Bi, but ore-barren quartz just shows an opposite trend. The contents of Sb, Sr, Zn and Ba in quartz increase gradually, but those of Ni, Mn, Ga and Bi decrease from the Potouqing fault westwards.

Sulphur isotopes

Statistic results from 81 sulphur isotope data (Liu Shinian, 1987) show that all the $\delta^{34}S$ values are positive, and vary in a narrow range, mostly within the range of +6‰ – +8‰. This implies that the sulphur was derived mainly from depth and underwent a relative homogenization stage, i.e., the sulphur has a close relation with semi-autochthonous anatexic granites.

Lead isotopes

Studies (Wang Jijun and Feng Wentao, 1991) show that 1) the lead belongs to primary ordinary normal lead; 2) the lead is cratonization crust lead, especially, its mean evolution curve is identical to the curve of gneiss, relatively close to mantle lead; and 3) the lead in the ore has the same origin as that in the Jiaodong Group gneiss.

Oxygen isotopes

Oxygen isotope data (Liu Shinian, 1987) show the $\delta^{18}O$ values of ore quartz veins vary over a narrow range, with a mean value of +14.19‰ and a variance of 1.23, but the average $\delta^{18}O$ value of wall-rock granite is +9.55‰ with a difference reaching +4.5‰, which is close to the difference value between vein quartz and granite. This implies their closely genetic relationship.

Carbon isotopes

As studied by Liu Shinian (1987), the $\delta^{13}C$ values of calcite in four ore samples range from −3.91‰ to −5.43‰, with a maximum difference value of 1.53‰ and a mean value of −4.77‰. This result coincides with that of endogenetic hydrothermal calcite studied by Addy ($\delta^{13}C$ values range from −1‰ to −13.9‰) and that of hydrothermal carbonate in North

America porphyry copper ores ($\delta^{13}C$ values range from $-2.6‰$ to $-5.9‰$).

Fluid inclusions

As studied by Liu Shinian (1987), the fluid inclusions in quartz from auriferous ores are rich in Na^+, K^+, Cl^-, SO_4^{2-}, CO_2, etc. and extremely high in salinity and mineralization degree, those in Au-poor quartz come next, and the lowest values are produced in those of gold-barren quartz, but the Eh values of fluid inclusions decrease with increasing gold content.

References

Chen Yanjing and Fu Shigu, 1992, Metallogenic rules of gold deposits in the West Henan region: Beijing, Seismological Press, p.108 – 121 (in Chinese).

Leading Office of Gold, Chinese Academy of Sciences, 1994, Progress in Gold Research of China: Beijing, Seismological Press, p.362 – 369 (in Chinese).

Liu Shinian, 1987, Geochemical research on ore-controlling faults in the Linglong gold ore field, Shangdong Province: Earth Science, v.1, n.12, p.39 – 48 (in Chinese).

Lu Guxian and Kong Qingcun, 1993, Geology of the Jiaojia-type gold deposit, Linglong area, East Shangdong: Beijing, Science Press, p.105 – 190 (in Chinese).

Wang Jijun and Feng Wentao, 1991, Features and ore-forming model of Linglong gold deposit: Contributions to Geology and Mineral Resources Research, v.6, n.2, p.18 – 35 (in Chinese).

Wu Xueyi, 1996, The characteristics and modelling experiments on the ore-controlling structure of shear zone-hosted gold deposits in China: Geotectonica et Metallogenia, v.20, n.1 – 2, p.31 – 33 (in Chinese).

Wu Xueyi and Yang Yuangen, 1994, Tectono-geochemical simulating experiments on Erjia gold deposit, Hainan Province: Geochemistry of Ore Deposits: Beijing, Seismological Press, p.41 – 46 (in Chinese).

Wu Xueyi, Yang Yuangen, Wang Zijiang, and Wu Huiming, 1992, Tectono-geochemical simulating experiments on Gaocun gold deposit of Hetai: Annual Report of Open Laboratory of Ore Deposit Geochemistry, Chinese Academy of Sciences: Beijing, Seismological Press, p.167 – 177 (in Chinese).

Wu Xueyi, Yang Yuangen, Xiao Huayun, and Wu Huiming, 1999, Geological characteristics of the main types of gold deposits in shear zones and simulating experiments on tectono-controlled gold mineralization: Geotectonica et Metallogenia, v.22, n.2, p.1 – 11 (in Chinese).